Nano Energy 37 (2017) 46–52

Contents lists available at ScienceDirect

Nano Energy

journal homepage: www.elsevier.com/locate/nanoen

Communication

Cross-conjugated oligomeric quinones for high performance organic batteries

Yan Jing[a], Yanliang Liang[a], Saman Gheytani[a], Yan Yao[a,b,*]

[a] Department of Electrical and Computer Engineering and Materials Science and Engineering Program, University of Houston, Houston, TX 77204, USA
[b] Texas Center for Superconductivity at the University of Houston, Houston, TX 77204, USA

ARTICLE INFO

Keywords:
Quinone
Oligomer
Cross-conjugation
Lithium-ion battery
Nanocomposite

ABSTRACT

Quinones with their structural diversity and electrochemical reversibility are among the most promising organic electrode materials. One distinct feature of quinones is their cross-conjugated structure, the importance of which in the design of organic electrode materials is so far overlooked. Here we report the design, synthesis, and characterizations of two cross-conjugated quinone oligomers (PBDTD and PBDTDS) and their nanocomposites with carbon nanotubes as potential low-cost organic electrode materials for Li-ion batteries. We investigate the effect of conjugation structure and molecular conformations (planar vs. helical) on electrochemical properties such as electronic conductivity, ionic conductivity, and electrode kinetics. Both quinones deliver similar specific capacity over 200 mA h g^{-1} at 2.5 V versus Li/Li^+ with excellent stability over 250 cycles. In particular, the difference in their rate performance is mainly determined by two aspects. First, cross-conjugation of PBDTD becomes electron transport-favorable through-conjugation after reduction, while PBDTDS is always cross-conjugated. Second, the planar conformation of PBDTD facilitates electron-transfer compared with the helical PBDTDS. This work provides insights into the popular yet less understood cross-conjugated quinone-based electrode materials and will stimulate the design of better quinone materials to achieve high-performance organic batteries.

1. Introduction

The increasing demand for energy is one of many challenges of the 21st century. Traditionally lithium-ion battery electrode materials have been limited to hard inorganic compounds [1–3]. Recently organic materials as redox-active electrode materials have attracted significant attention for energy storage due to their unique advantages in tunable redox properties, flexibility, low-cost, and environmental friendliness [4–6]. Compared to inorganic materials, organic compounds are composed of naturally abundant elements (C, H, N, O, S) and their redox-potential and specific capacity could be tailored through molecular structure design, providing almost unlimited choices [7]. Quinone compounds are one type of organic redox materials that have been widely studied due to their high specific capacity and electrochemical reversibility [8–11]. One major challenge for quinone small molecules is the high solubility of the active materials or lithiated compounds in the electrolyte, a common strategy is to incorporate quinone unit into polymer backbone or apply as a pendant group in a non-conjugated polymer [12]. For instance, Zhou and coworkers reported poly(anthraquinonyl sulfide) (PAQS) as a lithium-ion battery cathode material [13]. Nishide and coworkers reported poly(2-vinylanthraquinone) as an anode in a polymer/air battery [14]. Although several polymeric quinones have been successfully demonstrated previously, their cross-conjugated nature was not recognized as beneficial [9,13,15].

Fig. 1 illustrates three types of conjugation systems and corresponding examples. A through-conjugated system consists of alternating single and double bonds for electron delocalization. Through-conjugated compounds have been studied for battery electrodes since 1980s [16]. P-type conducting polymers such as poly(pyrrole), poly(thiophene), poly(aniline) have been investigated with high electronic conductivity [16,17]. However, the main drawback is the limited achievable degree of doping and unsatisfactory cycling stability caused by the repeated volume change due to anion insertion [17]. We recently demonstrated P(NDI2OD-T2) (Fig. 1) as a "conjugated redox polymer" that shows two electron reduction per repeating unit and 3000 stable cycles with 90% capacity retention, which expands the through-conjugated polymer library to include n-type conducting polymers [18]. A non-conjugated system is characterized by saturated bonds interrupting the conjugation, therefore electrons need to hop from one redox site to another. Non-conjugated

* Corresponding author at: Department of Electrical and Computer Engineering and Materials Science and Engineering Program, University of Houston, Houston, TX 77204, USA.
E-mail address: yyao4@uh.edu (Y. Yao).

http://dx.doi.org/10.1016/j.nanoen.2017.04.055
Received 19 February 2017; Received in revised form 8 April 2017; Accepted 26 April 2017
Available online 03 May 2017

compounds are typical electronic insulators therefore require significant amount of carbon additives to increase the electronic conductivity [19]. P(NDI2OD-TET) (Fig. 1) is an example of non-conjugated polymers.

A cross-conjugated compound is defined as possessing three unsaturated groups of which two are conjugated to a third but are not conjugated to each other. The unsaturated center is labeled with an asterisk as the bifurcation point [20]. Such a third unsaturated center can be either double bond or atoms with lone pairs of electrons in the $p\pi$ orbital [21], such as N, O, S, *etc*. In contrast to through-/non-conjugated structures, the value of cross-conjugated system is largely unrecognized. A possible explanation is that cross-conjugation is traditionally considered as less capable of promoting electron delocalization, thus exploiting cross-conjugation structure was considered not promising for efficient electron transport [20]. However, recent reports revealed different findings. Andrews et al. reported an 8 orders of magnitude increase in conductance for a cross-conjugated molecule during electrostatic doping [22]. It was found that enhanced electron delocalization occurred in the doped state as cross-conjugated radical ions improved electron conduction [23]. In addition, PAQS has also shown much better rate capability than a non-conjugated polyimide based electrode [15]. Although the underlying mechanism for the performance difference was not discussed in the paper, the cross-conjugated nature of PAQS should contribute to the faster electrode kinetics. Both reports indicate that cross-conjugated structures could be very useful in high-performance organic battery electrode materials.

In this work, we designed and synthesized two oligomeric hetero-aromatic-fused quinones and investigated the factors that influence their electrochemical properties for Li-ion storage. Fig. 1 show PBDTD (poly(benzo[1,2-b:4,5-b′]dithiophene-4,8-dione-2,6-diyl)) and PBDTDS (poly(benzo[1,2-b:4,5-b′]dithiophene-4,8-dione-2,6-diyl sulfide)) are composed of a benzo[1,2-*b*:4,5-*b′*]dithiophene-4,8-dione (BDTD) unit in the backbone. Both quinones share the poorly electronically conducting cross-conjugated structure due to the quinone building blocks and sp^3 sulfur atoms in the backbone. We have investigated the evolution of the conjugation structure of the quinones during charge-discharge and its impact on electrode performance. The insertion of sulfur atoms in between BDTD units modifies the molecular conformation from planar in PBDTD to helical in PBDTDS, offering an opportunity to investigate the influence of molecular conformation on electrode performance. We have also prepared nanocomposites of the quinones with carbon nanotubes (CNT) to optimize the morphology and maximize the energy/power density of the electrodes. Through a combined effort of theoretical simulation and electrochemical analysis, we provide insight into the influence of conjugation type and conformations on the electrode thermodynamics and kinetics of quinones for Li-ion storage.

2. Experimental section

2.1. Synthetic procedures of oligomeric quinones and CNT composites

2.1.1. Synthesis of 2,6-dibromobenzo[1,2-b:4,5-b′]dithiophene-4,8-dione (BrBDTDBr)

To a solution of benzo[1,2-*b*:4,5-*b′*]dithiophene-4,8-dione (BDTD) (500 mg, 2.27 mmol, Solarmer Materials Beijing Inc.) in trifluoroacetic acid (22.0 mL), N-bromosuccinimide (NBS) (2.530 g, 6.30 mmol) was added in a 50 mL round-bottom flask. The resulting clear yellow solution was refluxed at 115 °C, and monitored by TLC. After 24 h, the reaction was allowed to cool down and poured into 100 mL of deionized water and extracted by chloroform. Organic layer was collected and washed by hot THF and ethyl acetate and dried over reduced pressure. The product BrBDTDBr (707 mg, 1.87 mmol, 82.4% yield) was obtained as an orange powder, which was directly used in the next step without further purification. ^{1}H NMR (400 MHz, $CDCl_3$)δ 7.59 (s, 2H). IR (neat, cm^{-1}): 1655, 1416, 1383, 1265, 1046, 874, 844, 726, 582.

2.1.2. Preparation of PBDTDS

To a solution of BrBDTDBr (189 mg, 0.50 mmol) in anhydrous N-methyl-2-pyrrolidone (NMP, 1.4 mL) in a 15 mL of oven-dried Schlenk flask, anhydrous sodium sulfide (39 mg, 0.50 mmol) was added under Ar atmosphere. The resulting mixture was subject to oil bath and heated at 100 °C for overnight. The resulting product (110 mg, 0.44 mmol, 88.9% yield) was filtrated, washed several times with deionized water and acetone, then dried at 120 °C for 12 h. IR (neat, cm^{-1}): 1654, 1483, 1419, 1358, 1240,1156, 1085, 968, 874, 729, 662, 621. Elemental analysis cal. $C_{30}H_6O_2S_8Br_2$ with 6% of ash, C, 38.55; H, 0.65; S, 27.44. Found: C, 37.76; H, 0.61; S, 29.13. Average molecular weight of 879 g mol^{-1} is obtained from elemental analysis.

2.1.3. Preparation of PBDTDS@CNT

To a solution of BrBDTDBr (189 mg, 0.50 mmol) in anhydrous NMP (1.4 mL) in a 15 mL of oven-dried Schlenk flask, CNTs (25 mg) were added under Ar atmosphere. The resulting mixture was subjected to sonication (Branson 2800 ultrasonic) for 1 h. After addition of anhydrous sodium sulfide (39 mg, 0.50 mmol) into the mixture, the reaction was heated at 100 °C overnight. The suspension was centrifuged once cooled to room temperature, washed several times with deionized water and acetone, then dried under reduced pressure. The crude composite was then suspended into 10 mL of DMF and further sonicated for 1 h by a probe sonicator (Branson Sonifier S-450A). After centrifugation and drying at 120 °C for 12 h, PBDTDS@CNT composite was obtained (131 mg, 0.44 mmol, 87.3% yield). The content of CNT in PBDTDS composites are 19.1 wt%.

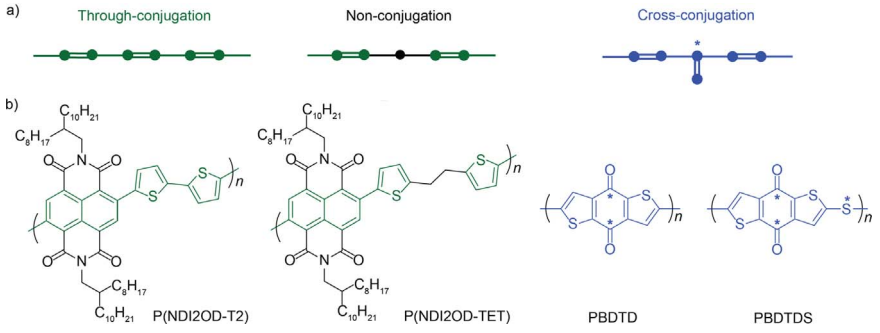

Fig. 1. Graphical illustration of three conjugation systems and corresponding molecular structures. **(**a) Through-conjugation (green), non-conjugation (black), and cross-conjugation (blue). (b) Corresponding molecular structures: P(NDI2OD-T2) for through-conjugation, P(NDI2OD-TET) for non-conjugation, PBDTD and PBDTDS for cross-conjugation. The asterisk (*) shows the bifurcation point in cross-conjugated molecules.

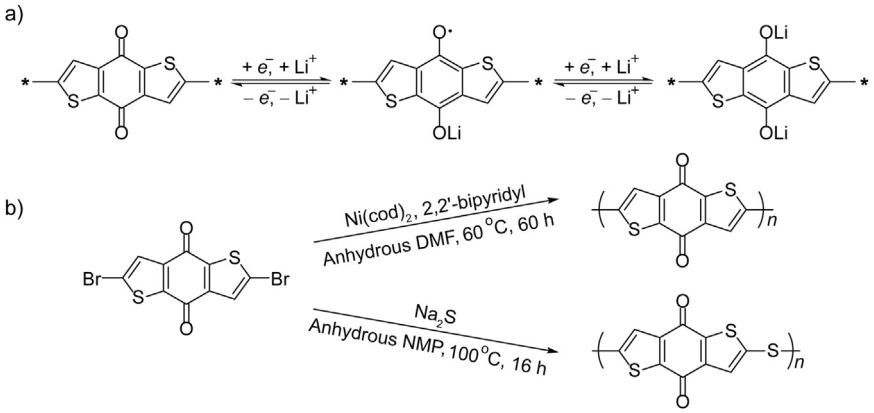

Fig. 2. (a) Two-step lithiation/delithiation mechanism of a BDTD-based quinone cathode; (b) Reaction routes and conditions for synthesizing PBDTD and PBDTDS, respectively.

2.1.4. Preparation of PBDTD

To a dark purple solution containing bis(1,5-cyclooctadiene) nickel(0), $Ni(cod)_2$, (216 mg, 0.78 mmol) and 2,2′-bipyridyl, 2,2′-bpy, (123 mg, 0.78 mmol) in dry DMF (11.0 mL) was added BrBDTDBr (189 mg, 0.50 mmol). The dark brown mixture was stirred for 60 h at 60 °C. The reaction mixture was poured into 1.0 M HCl (aq.), and the obtained brown powder was washed with 1.0 M HCl (aq.), an aqueous solution of disodium EDTA for three times, distilled H_2O, and methanol. The final crude product was further purified using a Soxhlet extractor with 50.0 mL of chloroform to afford brown powder (81 mg, 0.37 mmol, 74.3% yield). Elemental analysis cal. $Br(C_{10}H_2O_2S_2{\cdot}0.3DMF)_5Br$ with 2% of ash, C, 47.14; H, 1.49; S, 23.09. Found: C, 47.27; H, 1.56; S, 21.35. IR (neat, cm^{-1}): 1656, 1443, 1416, 1378, 1243, 1159, 1050, 1028, 872, 843, 763, 727. Average molecular weight of 1251 g mol^{-1} is obtained from elemental analysis.

2.1.5. Preparation of PBDTD@CNT

In a 25 mL of round-bottom flask, as-prepared PBDTD (25 mg) was dissolved in concentrated sulfuric acid (10 mL). To the above dark brown solution, 5.9 mg multiwall carbon nanotubes (OD: 5–15 nm, US Research Nanomaterials, Inc) were added into the suspension and stirred for 1 h so that both PBDTD and PBDTDS have the same CNT weight fraction. The suspension was then poured into 50 mL of deionized water and subjected to sonication (Branson 2800 ultrasonic) for 2 h. After centrifugation and drying at 120 °C for 12 h, PBDTD@CNT composite was obtained (30.9 mg, 100% yield). The content of CNT in PBDTD composites is 19.1 wt%.

2.2. Materials characterization

NMR spectra were recorded on a JEOL ECA–500 or ECX–400P spectrometer using residual solvent peak as an internal standard ($CDCl_3$: 7.26 ppm for ^1H NMR). IR spectra were performed as single reflection attenuated total reflectance measurements with powder samples using a Thermo Scientific Nicolet iS 5 instrument and iD 5 ATR accessory. Elemental analyses (EA) of polymer samples were performed by Midwest Microlab (Indianapolis, IN). Polymer molecular weights were determined on a Bruker Autoflex instrument. Scanning electron microscopy (SEM) was performed on a Gemini LEO 1525 microscope. Thermogravimetric analysis were conducted with TGA Q50. For the electronic conductivity measurement, pristine PBDTD(S) and PBDTD(S)@CNT powders were pressed into pellets with a diameter of 13 mm and 150–200 μm thick. Stainless steel foils were used as the contact in a two-terminal configuration and Keithley 2400 was used for the I-V measurement.

2.3. Electrochemical characterization

For the fabrication of Li-ion cells, composite electrodes containing PBDTD(S)@CNT were used as cathodes and metallic lithium was used as the anode. The contents of CNT in PBDTD(S) composites are both 19.1 wt%. A polypropylene membrane (Celgard) was used as a separator, and 1 M $LiClO_4$ in dioxolane-dimethoxyethane (1:1 v/v) as the electrolyte. A mixture containing 60 wt% composite, 30 wt% Super-P carbon, and 10 wt% polytetrafluoroethylene (PTFE) binder were hand-ground with pestle and mortar. The resulted films were pressed into stainless steel mesh with mesh size of 400×400 and wire diameter of 0.001 in. CR2032 coin cells were assembled in an Ar-filled glovebox (MBraun, Germany). Galvanostatic charge–discharge measurements was performed on a battery tester (CT2001A, LANHE). The specific capacity is calculated based on the mass of active materials. Electrochemical impedance spectroscopy (EIS) was performed on a potentiostat (VMP3, Biologic). Charge-transfer resistance (R_{ct}) were fitted with a $R_{el}(CPE(R_{ct}W_{dif}))$ equivalent circuit, where R_{el} is the electrolyte resistance, *CPE* is a constant phase element, W_{dif} is the Warburg impedance. Galvanostatic intermittent titration technique (GITT) was performed with cycled cells for 15 min discharge and rest 5 h or till voltage change less than 0.1 mV s^{-1}, respectively and at a discharge-charge rate of C/10. Calculations were performed with the Gaussian 09 program package using the B3LYP/6-31G(d, p) basis set.

3. Results and discussion

BDTD unit is a building block widely used in the synthesis of conjugated polymers for organic photovoltaic [24]. It was not investigated until 2013 when Chen and coworkers studied a series of fused heteroaromatic molecules including the BDTD molecule for organic batteries [25]. U. Schubert and coworkers recently reported the synthesis of poly(2-vinyl-4,8-dihydrobenzo[1,2-b:4,5-b′]dithiophene-4,8-dione) (PVBDT) as a pendant polymer via free radical polymerization method [26]. Although with higher molecular weight (M_n) of 2500–4700 Da, the pendant polymer still suffered a 50% capacity loss within 100 cycles.

Fig. 2a shows the reaction mechanism of BDTD during lithiation/delithiation. Each BDTD unit is reversibly reduced via a two-step process. Formation of an aromatic structure during reduction stabilizes the negatively charged carbon-oxygen groups, which are balanced by counter Li-ions from the electrolyte. We conducted DFT calculations to investigate the intramolecular energy for half-reduced BDTD–Li molecule in three different conformations shown in Fig. S1. The calculations are based on standard B3LYP/6-31G(d, p) basis-set. Fig. S1a shows the conformation where Li-ion solely coordinates to the negatively charged O atom with the lowest intramolecular energy. Fig. S1b shows Li-ions concurrent coordinate to both O and S atoms in forming a five-member ring conformation, which is less thermodyna-

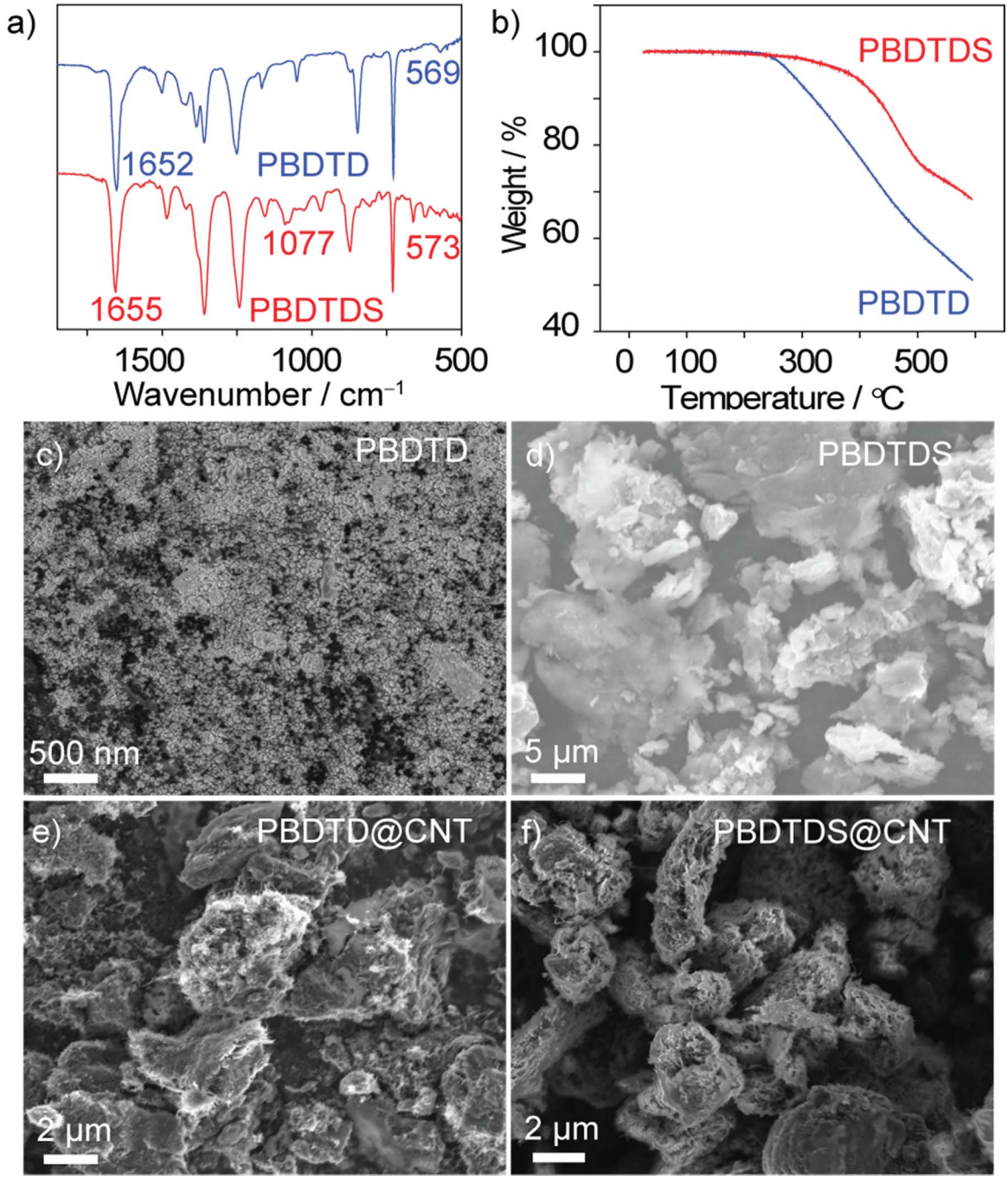

Fig. 3. (a) FTIR spectra of PBDTD and PBDTDS. (b) Thermogravimetric curves of PBDTD and PBDTDS in N_2 environment at a heating rate of 5 °C min^{-1}. (c-f) SEM images of pristine (c)PBDTD, (d) PBDTDS, and composites with (e) PBDTD@CNT, (f) PBDTDS@CNT, respectively.

mically favorable with additional energy (+0.435 eV). Fig. S1c shows Li-ions coordinate to the both O and H atoms in forming a six-member ring, which requires additional 1.607 eV in energy. Fig. 2b describes the synthetic routes used in this work. Briefly, brominated BDTD (BrBDTDBr) reacted with catalyst $Ni(cod)_2$ and ligand 2,2′-bipyridyl in dimethylformamide (DMF) at 60 °C for 60 h to afford PBDTD [27]. PBDTDS was synthesized by reacting BrBDTDBr with Na_2S in NMP at 100 °C for 16 h. Detailed synthetic procedures are described in the Section 2.

We investigated the chemical structure of as-synthesized quinones via attenuated total reflection Fourier transform infrared (ATR-FTIR) spectroscopy and elemental analysis (EA). As shown in IR spectra in Fig. 3a, the absorption peaks at 1652 and 1655 cm^{-1} are attributed to the stretching vibrations of carbonyl groups in PBDTD, PBDTDS, respectively; peaks at 569 and 573 cm^{-1} in fingerprint region are ascribed to the stretching vibrations of C–Br bonds, indicating the existence of C–Br as ending groups in both compounds. The absorption peaks at 1010–1100 cm^{-1} in the spectrum of PBDTDS are assigned to the stretching vibrations of C–S bond in between BDTD units [28]. EA was then conducted to determine elemental composition and as a tool to evaluate the average number of repeating units. EA results show that PBDTDS as a trimer and PBDTD as a pentamer with C–Br bond as ending groups. For simplicity, we still use PBDTD and PBDTDS to name the two quinones. The low degree of polymerization is attributed to the poor solubility of precursor and final products in the polymerization solvent. In addition, both quinones exhibit limited solubility in common solvents. Their poor solubility has prevented us from acquiring a ^{13}C NMR spectrum with meaningful signal. The thermal stability

of the quinones through thermogravimetric analysis (TGA) (Fig. 3b) shows the decomposition temperatures with 10% mass loss are at 319 °C and 431 °C for PBDTD and PBDTDS, respectively.

Scanning electron microscopy (SEM) images show the two pristine quinones have distinct morphology (Fig. 3c and d): the particle size of PBDTD (~50 nm) is much smaller than that of PBDTDS (~5 μm) due to the different polymerization condition used. Both quinones seem to be poorly crystallized, as is indicated by the lack of any well-defined diffraction peaks in their XRD patterns (Fig. S2). In order to conduct a fair comparison of performance, similar morphology of active materials is necessary. An effective method to modify morphology is to incorporate low-dimensional carbon nanostructures [15]. We employed CNTs as a structural scaffold to obtain quinone@CNT composites. In situ polymerization of PBDTDS in the presence of CNTs was adopted to synthesize PBDTDS@CNT. PBDTD@CNT was prepared by precipitating PBDTD from concentrated sulfuric acid to water in the presence of CNTs. As a result, fiber-like CNT/quinone nanocomposites were obtained with similar porous morphology (Fig. 3e and f).

Lithium coin cells were then fabricated to evaluate the electrochemical properties of the two BDTD-based quinones. The typical active material mass loading is 2–3 mg cm^{-2} for the tested electrodes. Galvanostatic charge–discharge measurements were conducted with a voltage range from 1.9 to 3.2 V vs. Li/Li^+ at C/10 (1 C=197.6 and 214.2 mA g^{-1} for PBDTDS trimer and PBDTD pentamer, respectively). As shown in Fig. 4a, PBDTDS and PBDTD can deliver specific capacity of 200 mA h g^{-1} at 2.56 V and 214 mA h g^{-1} at 2.52 V, respectively, corresponding to two electron reduction per unit in both cases. Both quinone oligomers show sloping voltage profiles, in sharp contrast to the flat plateau observed in BDTD molecules [25]. The two separate redox peaks are clearly visible in cyclic voltammograms in Fig. S3. The first reduction peak of PBDTD of 2.61 V is slightly lower than that of PBDTDS (2.72 V), and the second reduction peaks are very close (2.41 vs. 2.42 V). Similar to BDTD small molecule [25], the potential of PBDTD(S) are ~300 mV higher than anthraquinone-based compounds (PAQS, 2.2 V vs. Li/Li^+) due to the high-lying LUMO level of electron-rich BDTD unit.

Dissolution of active materials in organic electrolyte has been considered as a major challenge for organic electrodes. PBDTD barely dissolves in polar solvents (e.g. DMF, NMP) and only dissolves in concentrated sulfuric acid, while PBDTDS shows extremely poor solubility in all solvents. As a result, PBDTD demonstrated 96% of capacity retention after 250 cycles (Fig. 4b). For PBDTDS, the capacity first increased from 121 to 145 mA h g^{-1} in the first 50 cycles and 95% of the highest capacity is remained after 250 cycles. Such stability is a significant improvement from that of the previously reported PVBDT, composite electrodes of which containing 50–80 wt% of CNT conductive additives show 15–54% capacity retention after 100 cycles albeit with a higher molecular weight (M_n: 2500–4700 g mol^{-1}). This comparison implies that high molecular weight does not guarantee stable cycling. In fact, PVBDT is soluble in aprotic polar solvents such as DMF and NMP, while PBDTD is only slightly soluble and PBDTDS is extremely insoluble in these solvents. Therefore, designing intrinsically insoluble organic materials is particularly important for developing stable organic electrodes.

Furthermore, excellent rate performance was achieved in both quinone nanocomposites (Fig. 4c). PBDTD@CNT and PBDTDS@CNT showed 87.5% and 79.4% of capacity at 10 C compared to that at 1 C. Initial comparison of two pristine quinones found that PBDTD shows much better rate capability than that of PBDTDS (Fig. S4). However, their distinct particle sizes make it difficult to conclude whether the difference mainly comes from the morphology or as an intrinsic property. Formation of nanocomposites with CNTs makes the morphology of the quinones largely similar and at the same time improves the electrode kinetics. For instance, PBDTDS@CNT shows a capacity up to 131 mA h g^{-1} at 10 C compared to 42 mA h g^{-1} in bulk PBDTDS at the same rate (Fig. S4). Dramatically reduced particle size from PBDTDS to PBDTDS@CNT accounts for the improved rate capability. In contrast, the improvement with PBDTD@CNT relative to PBDTD is less significant: both electrodes show ~165 mA h g^{-1} at 10 C though the amount of conductive additives in PBDTD@CNT is only half of that

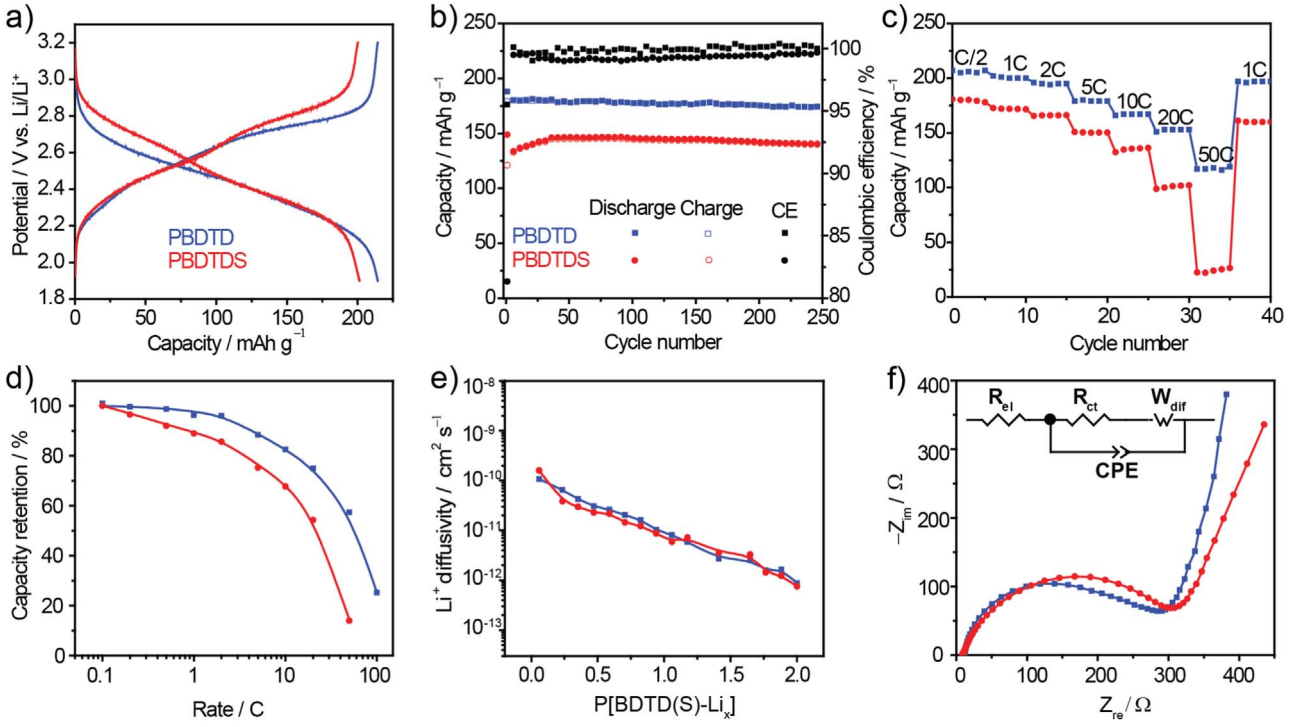

Fig. 4. Electrochemical characterizations of two quinone composite electrodes: PBDTD@CNT (blue) and PBDTDS@CNT (red). (a) The typical galvanostatic voltage profiles with a voltage cutoff of 1.9–3.2 V at 0.1 C. (b) Cycling stability at 5 C for 250 cycles. (c) Discharge specific capacity at various rates. (d) Discharge capacity retention at various rates, 0.1–50 C (PBDTDS@CNT), 0.1–100 C (PBDTD@CNT). (e) Li-ion diffusivity measurement using GITT method. (f) Nyquist plots for two quinone electrodes at fully charged state (3.2 V vs Li^+/Li). Inset shows an equivalent circuit.

in PBDTD. The extent of improvement is thus strongly correlated to the change of particle size before and after mixing with CNTs. It is helpful to recall that the original particle size of PBDTD (~50 nm) is much smaller than that of PBDTDS (~5 μm).

Even with similar morphology, the rate performance of PBDTD is still consistently superior to that of PBDTDS, which leads us to explore other performance-determining factors in quinone electrodes. We first determined Li^+ diffusion coefficients in the electrode using galvanostatic intermittent titration technique (GITT) [29]. As shown in Fig. 4e, two composite electrodes show similar Li^+ diffusivities in the range from 10^{-10} to 10^{-12} cm^2 s^{-1}, implying the ionic conductivity may not be the reason. Next, cyclic voltammetry is used to determine if the kinetics of electrode reaction is bulk diffusion limited or surface reaction limited. In Fig. S3c-d, current density at various sweep rates is fitted with the function $j=av^b$, where j is the measured current density, v is the potential sweep rate, a and b are constants. The fitted b values are between 0.92 and 0.96, indicating that the redox reactions of both electrodes are surface-limited instead of diffusion-controlled [30]. Furthermore, to quantitatively compare the electrochemical reaction kinetics, we adopted electrochemical impedance spectroscopy (EIS) to probe their charge transfer resistances (R_{ct}) [31]. Nyquist plots (Fig. 4f) exhibit similar size of semicircles at medium frequencies, i.e. 272.8 and 296.5 Ω for PBDTD and PBDTDS, respectively. All above results could not rationalize the observed difference in rate capabilities between PBDTD and PBDTDS.

We then conducted electronic conductivity measurements for pristine quinones and the composites (Table S1). Both pristine quinones are insulating in their intrinsic states, giving extremely low electronic conductivity values. The significant improvement in electronic conductivity from pristine quinones to composites is due to the incorporation of CNT. We expect the difference of electronic conductivity in two quinones to become significant only after reduction. However, it is technically difficult to measure the conductivity of reduced quinones: electrochemical reduction requires the use of conductive additives which obscure conductivity results, while chemical reduction is impeded by the poor solubility of both quinones in common solvents.

We further studied the influence coming from the conjugation structure of the quinones. Considering cross-conjugated molecules in reduced state would significantly promote charge delocalization compared to its neutral state [22], we examined the evolution of resonance structure in these two quinones during the charge/discharge process (Fig. 5a and b). Each cross-conjugated BDTD unit converts to a through-conjugated structure upon fully reduced. However, PBDTDS is always cross-conjugated due to the presence of S atoms as the bifurcation point even though the BDTD unit becomes through-conjugated. Therefore, the difference in the electronic structure in the discharged state between PBDTD and PBDTDS may lead to the difference in electronic conductivity, and thus different rate performance.

Molecular conformation and stacking could also play an important role in electronic conductivity. The presence of C–S–C bonds in PBDTDS allows the BDTD unit to rotate freely and achieve a most stable configuration with minimum energy; in contrast, the rotation of C–C bond between BDTD units in PBDTD is heavily restricted due to the adjacent C=C bonds in thiophene rings. To gain insight into the molecular conformation of PBDTD(S), we performed density functional theory (DFT) calculations [32]. Pentamers with C–Br as ending groups, i.e. $Br(BDTD)_5Br$ and $Br(BDTDS)_4BDTDBr$, were chosen as the model structures for PBDTD and PBDTDS, respectively. The optimized geometries are presented in Fig. 5c and d. $Br(BDTD)_5Br$ displays a planar conformation which favors π-π stacking and thus facilitates inter-molecular electron hopping. In comparison, the presence of C–S–C between BDTD units in $Br(BDTDS)_4BDTDBr$ results in a helical conformation with a ∠C–S–C angle of 102.8°. Such a geometry results in less efficient π-π stacking and unfavorable electron hopping. Moreover, the planar aromatic conformation in PBDTD could also incur better interactions between the quinone and CNT, making PBDTD@CNT a more “efficient” composite than PBDTDS@CNT. In addition, planar conformation is beneficial for extended electron delocalization than a helical one [33]. Therefore, the unique cross-conjugated structure and planar conformation of PBDTD is believed as

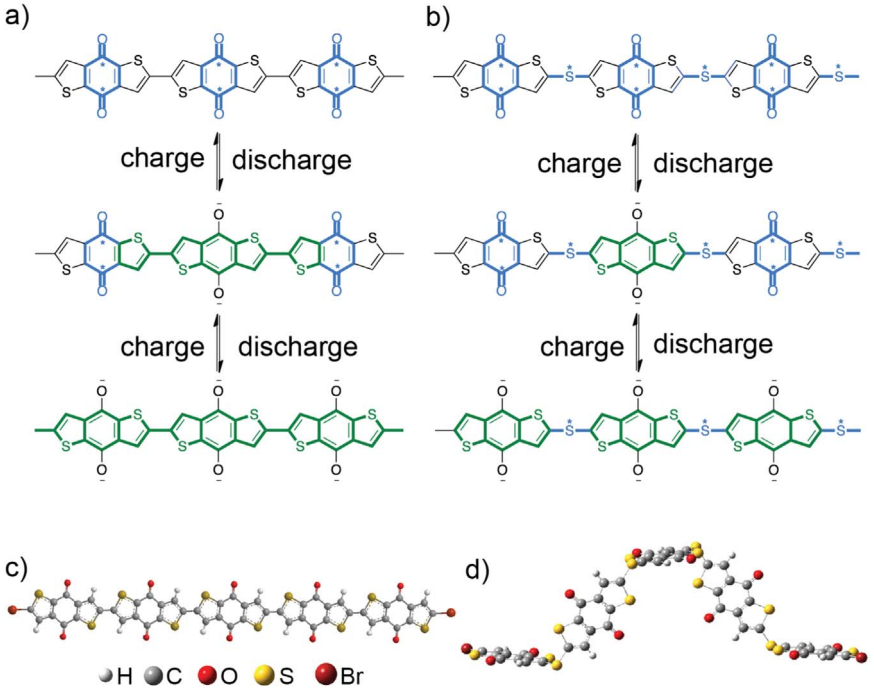

Fig. 5. (a-b) Conjugation evolution during the discharge/charge process. Asterisk * indicates the bifurcation point in BDT unit and at S atoms. In PBDTD, cross-conjugation (blue) evolves to through-conjugation (green) during lithiation. In PBDTDS, cross-conjugation (blue) remains during lithiation due to the bifurcation point at S atoms. (c-d) Optimized molecular conformations of PBDTD and PBDTDS using standard B3LYP/6-31G(d, p) calculations. Planar conformation of $Br(BDTD)_5Br$ and helical conformation of $Br(BDTDS)_4BDTDBr$.

main factors for the observed superior rate performance. To quantify the influence of conformation (or structure) on rate performance, the design of oligomers with similar conjugacy in all states, even more similar formulae, but different conformations (or with same conformation but different structures) would be more conclusive.

4. Conclusions

In summary, we report two cross-conjugated oligomeric quinones and evaluate them as organic cathode materials for lithium-ion batteries. Over 200 mA h g^{-1} of capacity is demonstrated for both quinones. Over 96% of capacity retention after 250 cycles indicates that heteroaromatic-fused oligomeric quinones could effectively suppress dissolution of active materials. Cross-conjugated PBDTD evolves to through-conjugation after fully discharge, which could significantly improve intra-chain electron conduction. Furthermore, DFT simulation reveals that PBDTD adopts a planar conformation which favors π-π stacking and hence inter-chain electron transport. As a result, PBDTD shows superior rate capability over the helical and always-cross-conjugated PBDTDS. This work provides insights into the popular yet less understood cross-conjugated quinone-based electrode materials and will stimulate new design principles of organic materials to achieve high-performance organic batteries.

Acknowledgements

Y.Y. acknowledges the funding support from the Advanced Research Projects Agency-Energy (DE-AR0000380), the Office of Naval Research Young Investigator Award (N00014-13-1-0543), the National Science Foundation (CMMI-1400261), the TcSUH core fund, and the University of Houston Startup fund. Y.J. acknowledges the computational support from the Center of Advanced Computing and Data Systems (CACDS) at the University of Houston.

Appendix A. Supporting information

Supplementary data associated with this article can be found in the online version at doi:10.1016/j.nanoen.2017.04.055.

References

[1] Z.S. Wu, G. Zhou, L.C. Yin, W. Ren, F. Li, H.M. Cheng, Nano Energy 1 (2012) 107–131.
[2] R. Mukherjee, R. Krishnan, T.M. Lu, N. Koratkar, Nano Energy 1 (2012) 518–533.
[3] J. Xu, S. Dou, H. Liu, L. Dai, Nano Energy 2 (2013) 439–442.
[4] Y. Liang, Z. Tao, J. Chen, Adv. Energy Mater. 2 (2012) 742–769.
[5] B. Huskinson, M.P. Marshak, C. Suh, S. Er, M.R. Gerhardt, C.J. Galvin, X. Chen, A. Aspuru-Guzik, R.G. Gordon, M.J. Aziz, Nature 505 (2014) 195–198.
[6] T. Janoschka, N. Martin, U. Martin, C. Friebe, S. Morgenstern, H. Hiller, M.D. Hager, U.S. Schubert, Nature 527 (2015) 78–81.
[7] B. Häupler, A. Wild, U.S. Schubert, Adv. Energy Mater. 5 (2015) 1402034.
[8] T. Ma, Q. Zhao, J. Wang, Z. Pan, J. Chen, Angew. Chem. Int. Ed. 55 (2016) 6428–6432.
[9] Z. Song, Y. Qian, X. Liu, T. Zhang, Y. Zhu, H. Yu, M. Otani, H. Zhou, Energy Environ. Sci. 7 (2014) 4077–4086.
[10] Z. Song, Y. Qian, M.L. Gordin, D. Tang, T. Xu, M. Otani, H. Zhan, H. Zhou, D. Wang, Angew. Chem. 127 (2015) 14153–14157.
[11] Y. Zhou, B. Wang, C. Liu, N. Han, X. Xu, F. Zhao, J. Fan, Y. Li, Nano Energy 15 (2015) 654–661.
[12] S. Muench, A. Wild, C. Friebe, B. Häupler, T. Janoschka, U.S. Schubert, Chem. Rev. 116 (2016) 9438–9484.
[13] Z. Song, H. Zhan, Y. Zhou, Chem. Commun. (2009) 448–450.
[14] W. Choi, D. Harada, K. Oyaizu, H. Nishide, J. Am. Chem. Soc. 133 (2011) 19839–19843.
[15] Z. Song, T. Xu, M.L. Gordin, Y.B. Jiang, I.T. Bae, Q. Xiao, H. Zhan, J. Liu, D. Wang, Nano Lett. 12 (2012) 2205–2211.
[16] P. Novák, K. Müller, K.S.V. Santhanam, O. Haas, Chem. Rev. 97 (1997) 207–281.
[17] A.G. MacDiarmid, Angew. Chem. Int. Ed. 40 (2001) 2581–2590.
[18] Y. Liang, Z. Chen, Y. Jing, Y. Rong, A. Facchetti, Y. Yao, J. Am. Chem. Soc. 137 (2015) 4956–4959.
[19] T. Nokami, T. Matsuo, Y. Inatomi, N. Hojo, T. Tsukagoshi, H. Yoshizawa, A. Shimizu, H. Kuramoto, K. Komae, H. Tsuyama, J. Yoshida, J. Am. Chem. Soc. 134 (2012) 19694–19700.
[20] P.A. Limacher, H.P. Lüthi, Wiley Interdiscip. Rev.: Comput. Mol. Sci. 1 (2011) 477–486.
[21] N.F. Phelan, M. Orchin, J. Chem. Educ. 45 (1968) 633–637.
[22] D.Q. Andrews, G.C. Solomon, R.P. Van Duyne, M.A. Ratner, J. Am. Chem. Soc. 130 (2008) 17309–17319.
[23] G.C. Solomon, D.Q. Andrews, R.H. Goldsmith, T. Hansen, M.R. Wasielewski, R.P. Van Duyne, M.A. Ratner, J. Am. Chem. Soc. 130 (2008) 17301–17308.
[24] J. Hou, M.H. Park, S. Zhang, Y. Yao, L.M. Chen, J.H. Li, Y. Yang, Macromolecules 41 (2008) 6012–6018.
[25] Y. Liang, P. Zhang, S. Yang, Z. Tao, J. Chen, Adv. Energy Mater. 3 (2013) 600–605.
[26] B. Häupler, T. Hagemann, C. Friebe, A. Wild, U.S. Schubert, ACS Appl. Mater. Interfaces 7 (2015) 3473–3479.
[27] K. Shiraishi, T. Yamamoto, Polym. J. 34 (2002) 727–735.
[28] A.S. Rahate, K.R. Nemade, S.A. Waghuley, Rev. Chem. Eng. 29 (2013) 471–489.
[29] Q. An, Y. Li, H.D. Yoo, S. Chen, Q. Ru, L. Mai, Y. Yao, Nano Energy 18 (2015) 265–272.
[30] X. Dong, L. Chen, J. Liu, S. Haller, Y. Wang, Y. Xia, Sci. Adv. 2 (2016) e1501038.
[31] M.D. Levi, G. Salitra, B. Markovsky, H. Teller, D. Aurbach, U. Heider, L. Heider, J. Electrochem. Soc. 146 (1999) 1279–1289.
[32] S. Er, C. Suh, M.P. Marshak, A. Aspuru-Guzik, Chem. Sci. 6 (2015) 885–893.
[33] C. Wang, Y. Xu, Y. Fang, M. Zhou, L. Liang, S. Singh, H. Zhao, A. Schober, Y. Lei, J. Am. Chem. Soc. 137 (2015) 3124–3130.

Yan Jing received his B.S. degree in Applied Chemistry from University of Science and Technology Beijing in 2011. He is pursuing Ph.D. in Materials Science and Engineering at the University of Houston. His research interests focus on developing organic redox materials for energy storage in aqueous and non-aqueous electrolytes.

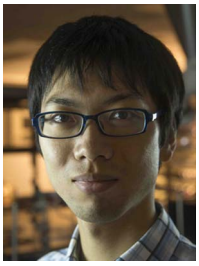

Yanliang Liang received his B.S. in 2007 and Ph.D. in 2012 from Nankai University, China, and is research associate in the University of Houston. His research interests are in the development of organic/hybrid materials for energy conversion and storage.

Saman Gheytani received his M.S. in Materials Science and Engineering from Sharif University of Technology, Tehran, Iran in 2009. He is pursuing the Ph.D. in Materials Science and Engineering at the University of Houston since 2013. His research interests include novel methods and materials for developing low-cost and safe aqueous rechargeable batteries for large-scale energy storage.

Yan Yao is an Assistant Professor of Electrical and Computer Engineering at the University of Houston. He received his Ph.D. in Materials Science and Engineering from UCLA in 2008. He worked at Polyera Corporation as a senior scientist and then a postdoctoral fellow at Stanford before joining the University of Houston in 2012. His research interests focus on magnesium/sodium ion batteries, aqueous batteries, and organic materials for energy storage. Yan received the Robert A. Welch Professorship in 2012, the Young Investigator Award from the Office of Naval Research (ONR) in 2013, the Ralph E. Powe Junior Faculty Enhancement Award from Oak Ridge Associated University in 2013, the Teaching Excellence Award from the College of Engineering in 2016, and the Scialog Fellow from the Research Corporation in 2017. Yan is the author and co-author of more than 60 peer-reviewed journal articles and 14 patent or patent applications.